arXiv:physics/9710042v1 [physics.chem-ph] 29 Oct 1997

Hybrid Quantum and Classical Mechanical Monte Carlo Simulations of the Interaction of Hydrogen Chloride with Solid Water Clusters

Darío A. Estrin [a,b], Jorge Kohanoff [b], Daniel H. Laria [a,c], and Ruben O. Weht [b,c]

[a] *Departamento de Química Inorgánica, Analítica y Química-Física e INQUIMAE, Facultad de Ciencias Exactas y Naturales, Universidad de Buenos Aires Ciudad Universitaria, Pabellón II, 1428, Buenos Aires, ARGENTINA.*

[b] *International Centre for Theoretical Physics Strada Costiera 11, 34014, Trieste, ITALY.*

[c] *Comisión Nacional de Energía Atómica, Avenida Libertador 8250, 1429, Buenos Aires, ARGENTINA.*

Monte Carlo simulations using a hybrid quantum and classical mechanical potential were performed for crystal and amorphous-like $HCl(H_2O)_n$ clusters ($n \leq 24$). The subsystem composed by HCl and one water molecule was treated within Density Functional Theory, and a classical force field was used for the rest of the system. Simulations performed at 200 K suggest that the energetic feasibility of HCl dissociation strongly depends on its initial placement within the cluster. An important degree of ionization occurs only if HCl is incorporated into the surface. We observe that local melting does not play a crucial role in the ionization process.

1 Introduction

Atmospheric chemistry is a research area in which many relevant processes occur in heterogeneous environments, such as the surface of solid particles and within liquid droplets. In particular, investigations connected with the stratospheric ozone layer have proved that ionic solvation of HCl at the surface of ice crystals is an important source of chlorine atoms, which may ultimately induce ozone-destroying chain reactions [1, 2, 3].

Simulations of HCl dissociation at ice surfaces using classical force fields have recently been reported [4, 5]. These are based on parametrizations of the potential energy surface which are derived from gas phase calculations for the isolated $HCl(H_2O)$ dimer and the ionic complex $Cl^- + H_3O^+$. Situations like those described above, in which a chemical reaction is strongly influenced by the environment, are rather delicate, and a purely classical approach risks of exhibiting problems of potentials transferability. A quantum mechanical semiempirical study has also been reported for HCl solvated in water clusters [6]. This calculation does take into account in a better way the effects of the environment, but it shows a very poor performance for the isolated HCl-acceptor water subsystem. This is a consequence of the limitations of the semiempirical description of the quantum mechanical Hamiltonian. Full *ab initio* Car-Parrinello simulations of HCl dissociation have been performed, although in a bulk water environment [7].

In order to use an accurate electronic structure technique and be able to sample adequately configuration space at an affordable computational cost, we have devised a hybrid approach [8, 9] in which the HCl-acceptor water subsystem is treated at the Density Functional Theory (DFT) level [10] and the rest of the system is modeled using the TIP4P potential for water [11]. We have also analyzed the role of the initial conditions and the local melting on the energetic feasibility of HCl dissociation in crystal-like and amorphous-like clusters $HCl(H_2O)_n$ ($n \leq 24$) at a temperature of 200 K using Monte Carlo simulation techniques.

2 The hybrid QM/CM strategy

The computational scheme is constructed by partitioning the system into a quantum mechanical (QM) and a classical mechanical (CM) region [8]. Considering N_c atoms in the classical subsystem with coordinates and partial charges $\{\mathbf{R}_i, q_i, i = 1, \cdots, N_c\}$ and N_q atoms in the QM region with coordinates and nuclear charges $\{\tau_\alpha, z_\alpha,\ \alpha = 1, \cdots, N_q\}$ the total energy can be written as:

$$E[\rho] = E_{\rm KS}[\rho] + \sum_{i=1}^{Nc} q_i \int \frac{\rho(\mathbf{r})}{\mid \mathbf{r} - \mathbf{R}_i \mid} \, {\rm d}\mathbf{r} + \sum_{i=1}^{Nc}\sum_{\alpha=1}^{Nq} [v_{\rm LJ}(\mid \mathbf{R}_i - \tau_\alpha \mid) + \frac{q_i z_\alpha}{\mid \mathbf{R}_i - \tau_\alpha \mid}] + E_{\rm CM} \ . \quad (1)$$

In this equation the first term is a purely quantum mechanical piece given by the standard Kohn-Sham expression [12]. The electronic density ρ is obtained by solving a Kohn-Sham set of equations self-consistently, where the external potential contribution to the Kohn-Sham operator includes the electrostatic interaction with the CM region, as given by the second and third terms of expression (1). The second term accounts for the electrostatic interaction of the charges representing the atoms (or molecules) situated in the CM region with the electronic charge distribution, while the third term corresponds to the Van der Waals and electrostatic interactions between the nuclei in the CM region and those in the QM region. TIP4P parameters [11] were used for O and H, and Lennard-Jones parameters for Cl were taken from [13]. The last term, E_{CM}, is the classical solvent contribution, and has been modeled with a flexible TIP4P potential for water which includes harmonic stretching and bending intramolecular terms extracted from extensive *ab initio* calculations [14]. The electrostatic interactions between nuclei in the QM region are included in the Kohn-Sham expression (first term).

For the QM region, computations are performed at the generalized gradient approximation (GGA) level. The correlation part is composed by the parametrization of the homogeneous electron gas due to Vosko [15] and the gradient corrections given by Perdew [16]. The local exchange term was supplemented with the gradient corrections proposed by Becke [17]. The exchange-correlation contribution to the potential and the energy is calculated by a numerical integration scheme based on grids and quadratures also proposed by Becke [18]. Gaussian basis sets are used for the expansion of the one-electron orbitals and also for

the additional auxiliary set used for expanding the electronic density. Double zeta plus polarization basis sets have been employed for Cl, O and H [19]. Auxiliary sets were also taken from Ref. [19].

In order to check the accuracy of the QM part of the Hamiltonian, geometry optimizations and vibrational analysis have been performed for isolated HCl, H_2O and $HCl(H_2O)$. Structural results are shown in Table 1, together with results recently obtained at the MP2 level [20]. The agreement between DFT-GGA and MP2 results as well as with available experimental data is rather satisfactory. This is consistent with previous work [21, 22] in which DFT calculations at the GGA level proved to perform well for hydrogen-bonded dimers.

The performance of the QM/CM approach was tested by computing the binding energies, structural parameters and vibrational frequencies of the clusters $HCl(H_2O)_n$ (n=2,3), considering the subsystem formed by HCl and the acceptor water molecule as the QM subsystem, and the remaining water molecules as the CM part. For these clusters, MP2 and also some experimental results are available. Selected structural parameters are shown in Table 1. The agreement with the MP2 computed values is again reasonable. An increase of the HCl and a decrease of the OCl bond length with cluster size can be observed, implying that the H-bond strength increases with the number of water molecules in the cluster.

Binding energies and the ν_{HCl} vibrational stretching frequencies for $HCl(H_2O)_n$ (n=2,3) are reported in Table 2, compared with experimental data and MP2 results. A red shift in the HCl stretching frequency is experimentally observed upon complexation with water molecules, and reproduced by theoretical calculations. This implies that proton transfer is increasingly favored in larger clusters. Interaction energies for the $HCl(H_2O)$ complex show a good agreement with MP2 calculations. Results for larger clusters show an overestimation of binding energies seemingly because of the use of a TIP4P classical potential parametrized for bulk water. However, the errors are expected to become less important for larger aggregates, as one approaches the bulk situation.

3 Monte Carlo simulations

Finite temperature properties were simulated using a Monte Carlo (MC) technique [27]. The MC moves consisted of random changes in the positions of all the particles simultaneously (including intramolecular solvent motions), with maximum displacements independent of their respective masses. The standard Metropolis sampling algorithm was used [28], and the maximum displacements were adjusted to give an overall acceptance ratio of about 50%. Ensemble averages were calculated over 15000 trial moves in all cases, after 4000 moves of equilibration. All simulations were carried out at 200 K, a temperature which is characteristic of stratospheric conditions.

We have considered the following situations:

1. $HCl(H_2O)$, hereafter referred as Case 1.

2. $HCl(H_2O)_{16}$ amorphous-like clusters. The initial conditions for these clusters have been obtained by running classical MC simulations at 200 K, in which the structure of the $HCl(H_2O)$ dimer was constrained during the course of the simulation. This was achieved by fixing the HCl bond length to 1.34 Å(Case 2A) and 1.90 Å(Case 2B), respectively. In case 2A, the HCl molecule remained at the periphery of the cluster, while in case 2B it was incorporated into the surface.

3. $HCl(H_2O)_{24}$ crystal-like clusters. The initial conditions were generated by isolating a fragment of two bilayers of hexagonal ice, composed by 25 water molecules, and replacing an appropriately oriented water molecule with an HCl. In the first case we replaced a water molecule situated in the outer layer (case 3A). In the second and third cases, the water molecule replaced was selected in the second layer (cases 3B and 3C). In case 3B, the orientation of the HCl molecule was chosen such that it was H-bonded to a water acceptor molecule located in the first layer, while in case 3C the HCl was H-bonded to a water molecule located in the second layer. These are typical configurations that are likely to be found during the ice growth process under stratospheric conditions [4].

Schematic views for cases 1, 2A, and 2B are shown in Figure 1, and for cases 3A, 3B, and 3C in Figure 2.

Radial distribution functions $g(r)$ for H-Cl, H-O(acceptor water) and Cl-O(acceptor water) are presented in Figure 3 for cases 1, 2A, and 2B and in Figure 4 for cases 3A, 3B and 3C. It can be observed that an important extent of ionization occurs in cases 2B, 3B and 3C, *i.e.* in those situations where the HCl is incorporated into the surface, instead of remaining as an adsorbate. The degree of ionization, however, is not complete. This can be seen in the first peak of $g(r)$ for H-O(acceptor water), which lies at about 1.2 – 1.3 Å, while the optimized HO bond distance in $[H_3O]^+$ is about 1.0 Å.

It can be observed in Figure 3 that no ionization occurs in case 2A, where the HCl peak in the $g(r)$ remains at about the equilibrium distance of the isolated HCl molecule. The different behavior observed in cases 2A and 2B can be explained in terms of the solvation of the products, which is determined basically by the initial conditions. $[H_3O]^+$ prefers trigonal coordination, and situations in which it acts as an acceptor in H-bonds are unfavorable. On the other hand, Cl^- prefers maximum H coordination. In case 2B, $[H_3O]^+$ would be trigonally coordinated as well as the chloride ion, but in case 2A the chlorine is found in the periphery of the cluster and solvation is rather poor.

Figure 4 shows that there is no dissociation in case 3A. This is because Cl results with only coordination 2 and $[H_3O]^+$ would act as an acceptor of an H bond (tetrahedral coordination). In both 3B and 3C cases dissociation occurs. The larger degree of ionization observed in Case 3B is due to the fact that, while Cl always exhibits a trigonal coordination, in case 3C the $[H_3O]^+$ is tetrahedrally solvated, and in 3B it has the optimal trigonal coordination. It is also interesting to remark the different behavior observed for the $g(r)$ for O-Cl in the different simulations. In the case in which HCl is in the outer layer (case 3A), it peaks at about 3.00 Å and in cases in which it is in the second monolayer (3B and 3C), it peaks at 2.76 Å and 2.77 Å, respectively. The same trend is observed in the amorphous-like clusters (2A and 2B), for which $g(r)$ peaks at a larger value when HCl is not dissociated.

Ensemble averages for Cl Mulliken population, H-Cl, H-O(acceptor water), Cl-O(acceptor water) distances and binding energies are given in Table 3. More negative averages for the Cl Mulliken populations are consistent with the large degree of dissociation observed in cases 2B, 3B and 3C. It can also be noted that larger average binding energies per molecule are associated with the better solvated (larger extent of ionization) situations. In all simulations the clusters remained solid-like, at least in the region of phase space sampled during our simulations. Values of Lindemann's relative rms bond length fluctuations were typically 0.02. Melting phenomena have not been observed, even in the simulations with an important degree of dissociation.

4 Conclusions

We conclude that the energetic feasibility for HCl ionization in solid-like clusters strongly depends on the initial placement of the HCl within the system, which in turn determines the solvation properties of the products. Local melting phenomena turn out not to be necessarily related to the dissociation process. Our results on crystal-like clusters reinforce the conclusions of Ref. [4], in which simulations of HCl incorporated into bulk-ice surfaces were performed using classical potentials. Moreover, we have shown that the same conclusion holds for amorphous-like clusters. In the case of HCl adsorbed on top of ice surfaces it appears that the HCl dissociation process would not be energetically favorable [5]. These observations also show that the accuracy of the Hamiltonian description plays a fundamental role in these studies. The QM/CM Monte Carlo scheme proposed in this work provides an accurate tool for modeling chemical reactions in heterogeneous environments.

Before closing this article, we would like to make a final comment concerning ergodicity and proper sampling of all relevant fluctuations. During our MC runs the systems remained well-equilibrated and we did not observe any signature of transitions between the different solvation structures described in the previous paragraphs. This clearly shows the presence

of a high free energy barrier - in comparison to normal thermal energies - implying that, in principle, the feasibility of the dissociation process would be strongly dependent on the initial solvation conditions, *i.e.* on the details of the growth process. In any event, one would tend to believe that the more energetically favorable configuration, namely the one with the larger negative solvation energy (2B or 3B in our studies, see Table 3) would correspond to the most stable configuration from the thermodynamic point of view. However to be certain, a more complete analysis involving the computation of relative free energies between the different solvation structures is necessary; this would allow us to estimate not only equilibrium information but also information about rates of interconvertion between different solvation structures. Work in this direction is currently being undertaken.

Acknowledgments

D.A.E. acknowledges Fundación Antorchas and Universidad de Buenos Aires for financial support and ICTP for hospitality. We thank also Francesco Sciortino for providing us with ice configurations and Roberto Fernández Prini for bringing this problem to our attention and for useful discussions.

References

[1] J.P.D. Abbat and M.J. Molina, J. Phys. Chem. 96 (1992) 7674.

[2] M.J. Molina, T.L. Tso, L.T. Molina, and E.Y. Yang, Science 238 (1987) 1253.

[3] D.R. Hanson and A.R. Ravishankara, J. Phys. Chem. 96 (1992) 2682.

[4] B.J. Gertner and J.T. Hynes, Science 271 (1996) 1563.

[5] S.H. Robertson and D.C. Clary, J. Chem. Soc. Faraday Discussions, 100 (1995) 309.

[6] R. Buesnel, I.H. Hillier, and A.J. Masters, Chem. Phys. Lett. 247 (1995) 391.

[7] K. Laasonen and M.L. Klein, J. Am. Chem. Soc. 116 (1994) 11620.

[8] L.L. Ho, A.D. MacKerell Jr., and P.A. Bash, J. Phys. Chem. 100 (1996) 4466.

[9] D.A. Estrin, L. Liu, and S.J. Singer, J. Phys. Chem. 96 (1992) 5325.

[10] D.A. Estrin, G. Corongiu, and E. Clementi, in: METECC, Methods and Techniques in Computational Chemistry, ed. Clementi, E. (Stef, Cagliari, 1993) chapter 12.

[11] W.L. Jorgensen, J. Chandrasekar, J.D. Madura, R.W. Impey, and M.L. Klein, J. Chem. Phys. 79 (1983) 926.

[12] W. Kohn and L.J. Sham, Phys. Rev. A 140 (1965) 1133.

[13] M.P. Allen and D.J. Tildesley, Computer simulations of liquids (Clarendon Press, Oxford, 1987).

[14] R.J. Bartlett, I. Shavitt, and G.D. Purvis, J. Chem. Phys. 71 (1979) 281.

[15] S.H. Vosko, L. Wilk, and M. Nusair, Can. J. Phys. 58 (1980) 1200.

[16] J.P. Perdew, Phys. Rev. B, 33 (1986) 8822; Erratum, Phys. Rev. B 34 (1986) 7406.

[17] A.D. Becke, Phys. Rev. A 38 (1988) 3098.

[18] A.D. Becke, J. Chem. Phys. 88 (1988) 1053.

[19] N. Godbout, D. R. Salahub, J. Andzelm, and E. Wimmer, Can. J. Chem. 70 (1992) 560.

[20] M.J. Packer and D.C. Clary, J. Phys. Chem. 99 (1995) 14323.

[21] F. Sim, A. St-Amant, I. Papai, and D.R. Salahub, J. Am. Chem. Soc. 114 (1992) 4391.

[22] D.A. Estrin, L. Paglieri, G. Corongiu, and E. Clementi, J. Phys. Chem. 100 (1996) 8701.

[23] K.P. Huber and G. Herzberg, Molecular Spectra and Molecular Structure (Van Nostrand Reinhold, New York, 1979), Vol. IV.

[24] A.C. Legon and L.C. Willoughby, Chem. Phys. Lett. 95 (1983) 449.

[25] C. Amirand and D. Maillard, J. Mol. Struct. 176 (1988) 181.

[26] B.S. Ault and G.C. Pimentel, J. Phys. Chem. 77 (1973) 57.

[27] R.O. Weht, J. Kohanoff, D. A. Estrin, and C. Chakravarty (submitted).

[28] N. Metropolis, A.W. Rosenbluth, M.N. Rosenbluth, A.H. Teller and E. Teller, J. Chem. Phys. 21 (1953) 1087.

Figure Captions

Figure 1:
Schematic view of initial conditions. $HCl(H_2O)$ (Case 1) and $HCl(H_2O)_{15}$ (Cases 2A and 2B). Only H in the QM subsystem are shown. Relevant H bonds are represented with dashed lines.

Figure 2:
Schematic view of initial conditions. $HCl(H_2O)_{24}$ (Cases 3A, 3B and 3C). Only H in the QM subsystem are shown. Relevant H bonds are represented with dashed lines.

Figure 3:
H-Cl (solid line), H-O(acceptor water) (dashed-dotted line) and Cl-O(acceptor water) (dashed line) radial correlation functions, for cases 1, 2A and 2B. (distances in $\mathring{A}$)

Figure 4:
H-Cl (solid line), H-O(acceptor water) (dashed-dotted line) and Cl-O(acceptor water) (dashed line) radial correlation functions, for cases 3A, 3B and 3C. (distances in $\mathring{A}$)

TABLE 1: Selected optimized geometrical parameters for HCl, H_2O and $HCl(H_2O)_n$ (n=1,3) with bond lengths in Å and angles in deg. <OHCl is the hydrogen bond angle and dO···Cl and dO···H the hydrogen bond lengths.

		DFT [a]	MP2 [b]	MP2 [c]	Exp.
HCl	d HCl	1.286	1.271	1.281	1.275 [d]
H_2O	d HO	0.981	0.961	0.968	0.958 [d]
	<HOH	104.8	103.5	104.8	104.5 [d]
$HCl(H_2O)$	d HCl	1.320	1.287	1.302	
	d O ··· Cl	3.095	3.196	3.120	3.2149 [e]
	d O ··· H	1.776	1.910	1.818	
	<OHCl	176.6	176.7	178.7	
$HCl(H_2O)_2$	d HCl	1.343	1.303	1.326	
	d O ··· Cl	2.992	3.059	2.993	
	d O ··· H	1.672	1.787	1.688	
	<OHCl	165.6	163.3	166.5	
$HCl(H_2O)_3$	d HCl	1.369	1.323		
	d O ··· Cl	2.923	2.976		
	d O ··· H	1.558	1.657		
	<OHCl	174.2	174.7		

[a] this work.
[b] 6-31g(2dp) results of Ref. [20].
[c] Pol1 results of Ref. [20].
[d] Ref. [23].
[e] Ref. [24].

TABLE 2: Binding energies (kJ/mol) and ν_{HCl} stretching frequencies (cm^{-1}) for HCl and $HCl(H_2O)_n$. (n=1,3) [a]

		DFT [b]	MP2 [c]	MP2 [d]	Exp.
HCl	ν_{HCl}	2967	3068	2982	2991 [e]
$HCl(H_2O)$	ν_{HCl}	2512	2841	2709	2659 [f]
					2540 [g]
	ΔE_e	23.71	21.97	20.57	
	ΔE_o	14.18	13.74	10.93	
$HCl(H_2O)_2$	ν_{HCl}	2257	2615	2394	2390[f]
	ΔE_e	67.79	51.27	50.95	
	ΔE_o	50.04	30.53	32.86	
$HCl(H_2O)_3$	ν_{HCl}	2015	2341		
	ΔE_e	118.04	89.07		
	ΔE_o	89.00	54.70		

[a] ΔE_e is the cluster dissociation energy, ΔE_o includes also zero point energy corrections.
[b] this work.
[c] 6-31g(2dp) results of Ref. [20].
[d] Pol1 results of Ref. [20].
[e] Ref. [23].
[f] experimental results in Ar matrix (Ref. [25]).
[g] experimental results in N_2 matrix (Ref. [26]).

TABLE 3: Ensemble averages of Cl Mulliken population, H-Cl, H-O(acceptor water), Cl-O(acceptor water) bond distances (Å), and binding energy per molecule (kJ/mol). Values in parenthesis are standard deviations.

	qCl	d H-Cl	d H-O	Cl-O	E
1	-0.208 (0.017)	1.314 (0.026)	1.914 (0.118)	3.185 (0.107)	-7.7 (1.5)
2A	-0.245 (0.017)	1.325 (0.027)	1.752 (0.066)	3.061 (0.057)	-34.0 (0.6)
2B	-0.528 (0.036)	1.496 (0.047)	1.298 (0.052)	2.789 (0.039)	-36.6 (0.7)
3A	-0.280 (0.017)	1.344 (0.030)	1.672 (0.068)	2.997 (0.068)	-34.4 (0.4)
3B	-0.546 (0.027)	1.510 (0.040)	1.257 (0.037)	2.760 (0.043)	-35.9 (0.5)
3C	-0.464 (0.032)	1.440 (0.040)	1.335 (0.049)	2.769 (0.043)	-34.6 (0.6)

Figure 1

1

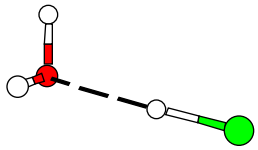

2A

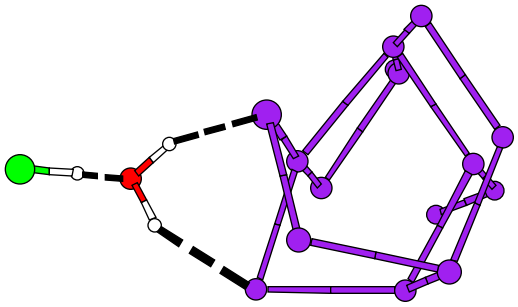

2B

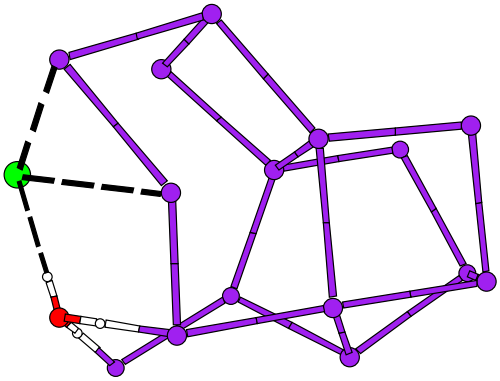

Figure 2

3A

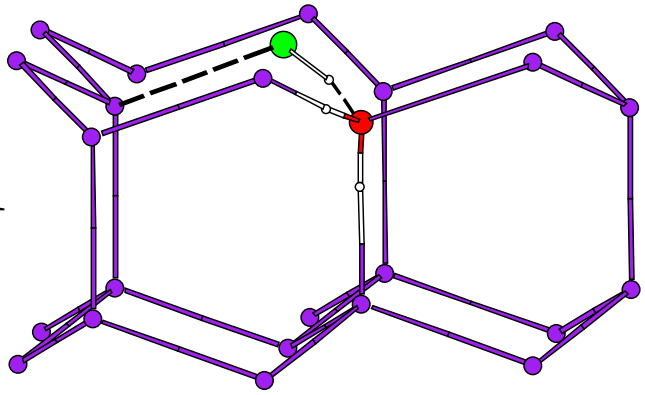

3B

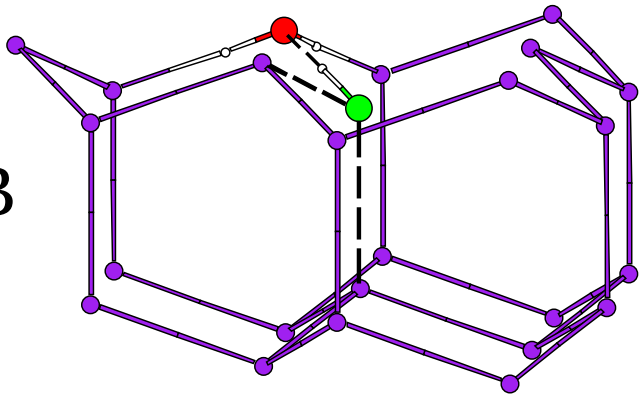

3C

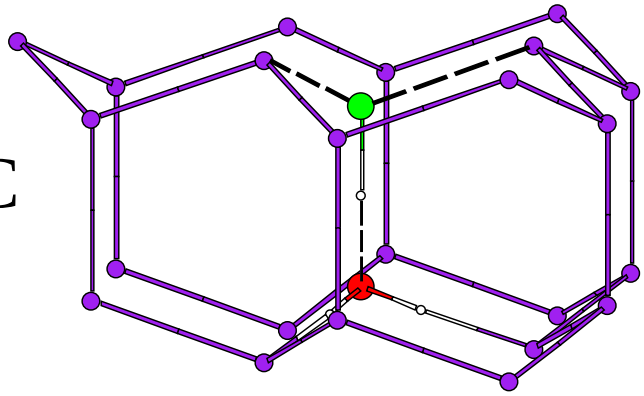

Figure 3

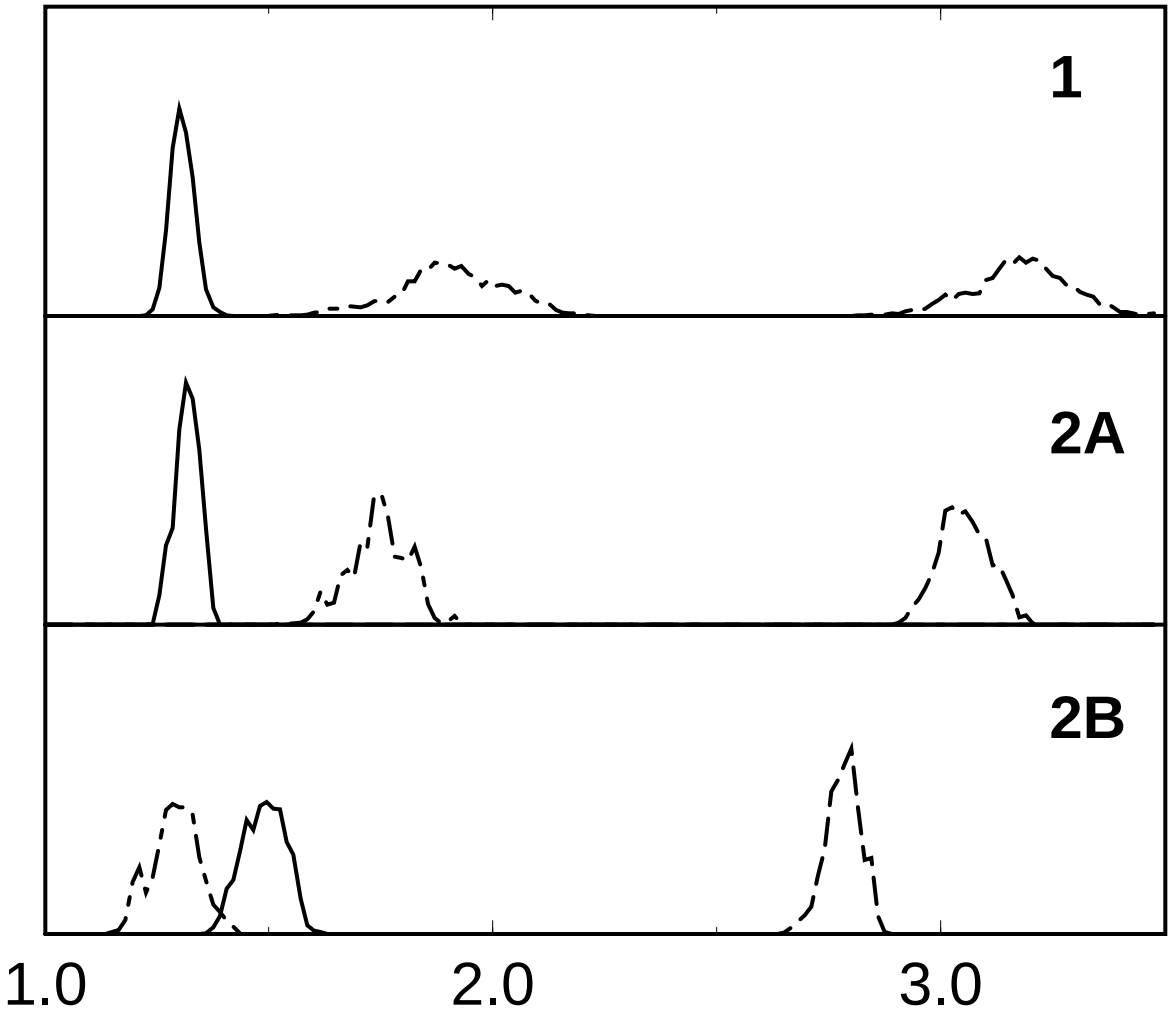
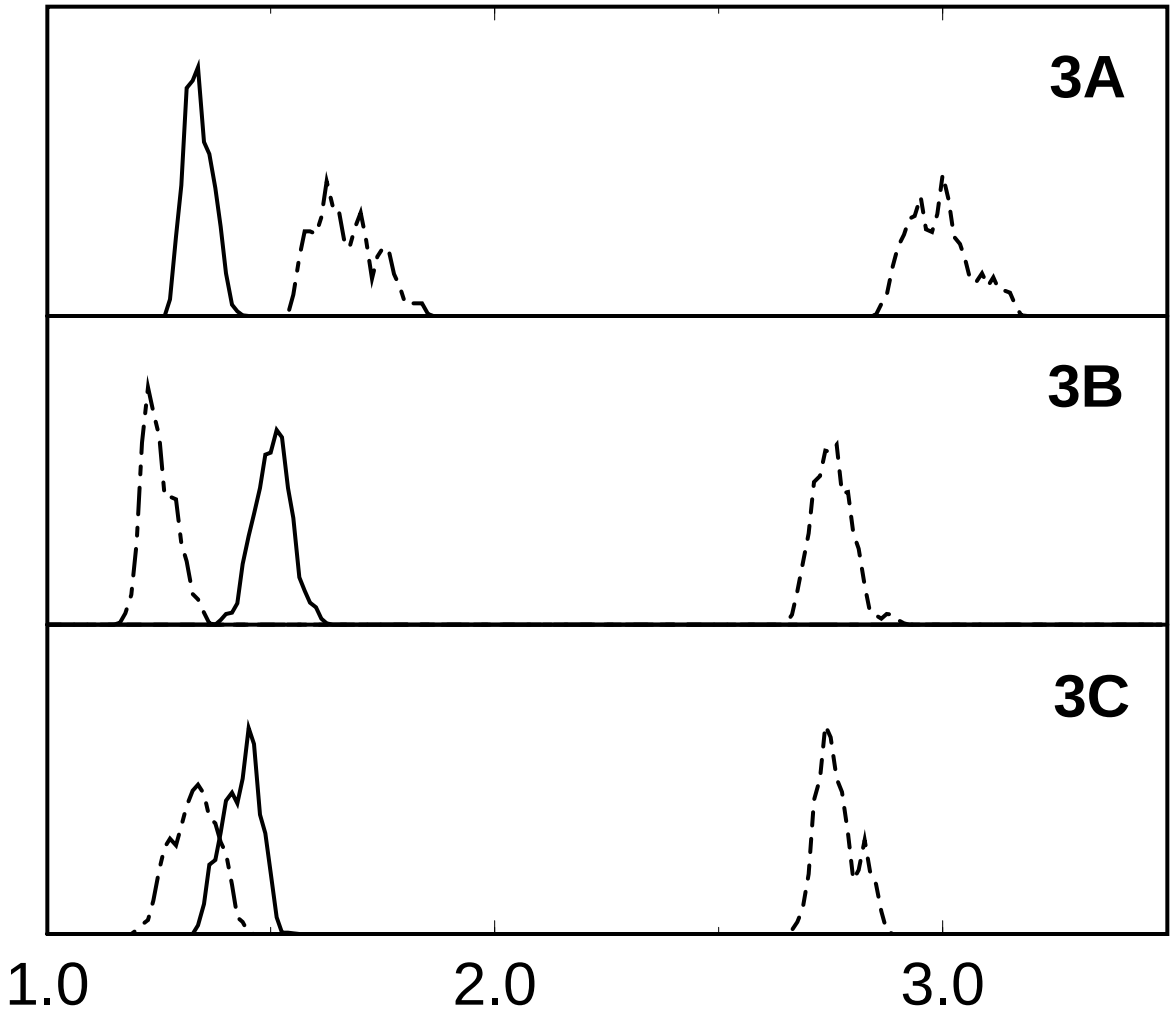
Figure 4